Hindawi Publishing Corporation
International Journal of Antennas and Propagation
Volume 2016, Article ID 2906149, 18 pages
http://dx.doi.org/10.1155/2016/2906149

Research Article

Design and Development of a New Electrically Small 3D UHF Spherical Antenna with 360° of Opening Angle in the Whole Space for RFID, WSN, and RSN Applications

Abdelhamid Bou-El-Harmel, Ali Benbassou, and Jamal Belkadid

Laboratory of Transmission and Processing Information Eq. EMC/Telecom, Sidi Mohamed Ben Abdullah University, High School of Technology, Road IMOUZZER, 2427 Fez, Morocco

Correspondence should be addressed to Abdelhamid Bou-El-Harmel; abdelhamid.bouelharmel@usmba.ac.ma

Received 16 August 2016; Revised 24 October 2016; Accepted 25 October 2016

Academic Editor: Sotirios K. Goudos

Several antenna designs have been made in order to obtain a novel electrically small 3D UHF spherical antenna (ka = 0.1916), which has a resonance frequency close to 915 MHz, produces a quasi-isotropic radiation with an opening angle equal to 360° in the whole space, and is used for RFID, WSN, and RSN applications. These antennas are based on different shapes and are wrapped on the Styrofoam sphere surface of dielectric constant close to air (ε_r = 1.06). A T-match configuration is used to adapt the input impedance of antennas to a value of 50 Ω. The antennas form allows for placing the sensor electronics in its interior, to reconfigure it for numerous values of impedances and to operate it in other ISM bands by adjusting their geometric parameters.

1. Introduction

The RFID sensor network (RSN) is an important wireless networking technology which belongs to Wireless Personal Area Network (WPAN). It forms a new research area, which solicited the interest of both the industry and the research community. This new technology is the result of the integration of the radio frequency identification (RFID) technology [1] and wireless sensor network (WSN) technology [2]. The integration of these two technologies can extend the range of applications and offer a benefit to existing applications [3–7]. Several implementations of this integration framework have been successfully performed and described in [8, 9].

The RSN architectures are possible architectures of the integrated RFID and WSN; according to research works [3–7], there are the four types of integrations class:

(i) Integration of RFID tags with sensors.

(ii) Integration of RFID tags with sensors WSN nodes.

(iii) Integration of RFID readers with WSN sensor nodes.

(iv) Mix of RFID and WSN.

In RFID, WSN, and RSN applications, the antenna is a fundamental and an essential element in the wireless communication between devices. There are many types of antennas operating at UHF frequencies located below the GHz, used in tags with or without sensor integrated, sensor nodes, and tags with sensor nodes integrated, such as the planar antennas [10, 11] and the three-dimensional (3D) antennas [12–15]. Regarding the planar antennas, they will always determine the size of the devices in contrary to 3D antennas, which allow the electronics sensor to be housed in its interior and occupy the majority of the overall volume of the devices, so these 3D antennas give us a reduced size of devices compared to planar antennas.

In the RFID system, an unread tag can cause a significant economic loss or threat to security [16]. In the literature, this nonreading problem can be solved by two ways:

(i) The use of multiple reader antennas [17]: but the reader antenna diversity is not always possible or sufficient.

(ii) The use of tags with two dipoles orthogonally placed [18]: but it requires a special chip circuit to provide a connection with two independent RF inputs.

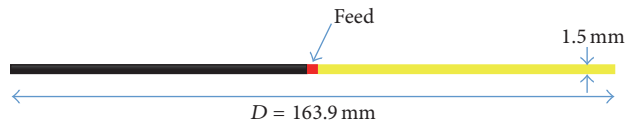

Figure 1: Structure of the half-wave dipole.

Regarding the WSN and RSN systems, we find the problem of intermittent communication between network nodes due to the use of dipole or monopole antennas, because the radiation pattern of the two antennas has zeros along its wire axis. In the zero direction, the information does not attain the node and the retransmission of information may cause a significant loss of energy, which leads to a reduction of the node lifetime.

So, the optimal solution of these problems is to use an antenna that produces a quasi-isotropic radiation pattern; that is, a radiation covers all directions of space (4π).

In previous works, the authors in [12] have designed an antenna for a spherical surface with a near-isotropic radiation pattern. The antenna is designed for wireless, UHF RFID sensors. It is electrically small (ka = 0.49 at the frequency of 915 MHz) with a diameter of 52 mm (radius = 26 mm) and operates in the UHF RFID frequency band. The antenna consists of two spherical-cap dipoles perpendicular between them and of spherical ABS plastic shell that was assumed to have a relative permittivity of 2.8 and a loss tangent of 0.01. According to the simulations, the antenna resonates at the frequency of 930 MHz with a minimum and maximum gain of 1.81 dBi and −8.07 dBi, respectively. In [13], the authors propose an electrically small spherical UHF RFID tag antenna with quasi-isotropic radiation patterns for potential applications in wireless sensor networks. The dipole antenna of 216 mm total length is packed onto a sphere's surface (Styrofoam), where the diameter of the sphere is 25 mm and the electrical size is a ka of 0.24. The antenna is designed at 911.25 MHz for a Korean UHF RFID band. A short stub is used to match with a micro RFID chip impedance. According to the simulations, the minimum return loss is −15.9 dB at 912 MHz, and the radiation pattern is quasi-isotropic with a maximum gain of 0.75 dBi.

Our goal in this work will focus on the contribution of the development of RFID, WSN, and RSN technologies based on several UHF 3D spherical antenna designs in order to obtain an electrically small 3D spherical antenna with a quasi-isotropic radiation and an opening angle equal to 360° used for tags with or without integrated sensors, sensor nodes, and tags with integrated sensor nodes. These latest devices can communicate only at the frequencies that belong to the allocated bands to industrial, scientific, and medical applications; these bands are called ISM bands. So, we have chosen the 915 MHz frequency as the operating one of the antenna which belongs to the ISM band [902–928 MHz].

Note that the design and the simulation were performed using the 3D electromagnetic simulator, HFSS (High Frequency Structure Simulator) which is based on the finite element method (FEM). The use of this simulator has helped us study the geometrical parameters of the antenna to determine the effect of each parameter and to determine an optimal value for each. The simulation results are compared by the CST Microwave Studio simulator (Computer Systems Technology) which is based on the finite integration technique (FIT). A slight difference between the results obtained by the two simulators is due to the difference between the numerical method of each simulator with the simulation step and the mesh used during the simulation.

Table 1: Dimensions of the T-match (Figure 4).

Parameters	$L1$	$L2$
Values (mm)	2.8	21.8

2. Antennas Design

In this section, we will design several antennas in order to find a very small antenna that operates approximately at 915 MHz and produces quasi-isotropic radiation with an opening angle of 360° in all directions of space. The starting point for these designs is a half-wave planar dipole antenna of total length D = 163.9 mm which corresponds to $\lambda/2$ in air at 915 MHz as presented in Figure 1.

We have chosen this antenna because it has omnidirectional radiation pattern with zeros along its axis wire even though its electrical size ka is greater than 0.5, where k is the wave number in free space $2\pi/\lambda$ and a is the radius of an imaginary sphere circumscribing the maximum dimensions of the antenna [19]. Then, it must cancel all zeros and reduce ka and that is the goal of the first design. So, we must cancel all zeros and reduce ka and that is the goal of the first design.

2.1. 3D Spherical Antenna Based on a Planar Dipole. In this design, we will wrap the dipole around the surface of a sphere as illustrated in Figure 2 so that the dipole takes the spherical form which gives us a reduction of ka and so that the current circulates in the same direction of the two arms of the dipole in a circular manner which gives us a quasi-isotropic radiation.

The used sphere is a Styrofoam sphere of dielectric constant close to the air (ε_r = 1.06) with a radius r = 26.34 mm which depends on D. We left a distance d = 1.5 mm so that we do not have an intersection between the arms.

The return loss $S11$ simulated by HFSS and CST of this antenna with the output impedance of the generator Z_g = 50 Ω is shown in Figure 3. We observe that the antenna has a greater $S11$ than −10 dB. Then, this winding of the dipole causes a mismatch of impedances. Thus, in order to adapt them, we used the T-match method as shown in Figure 4. The dimensions of this configuration are illustrated in Table 1.

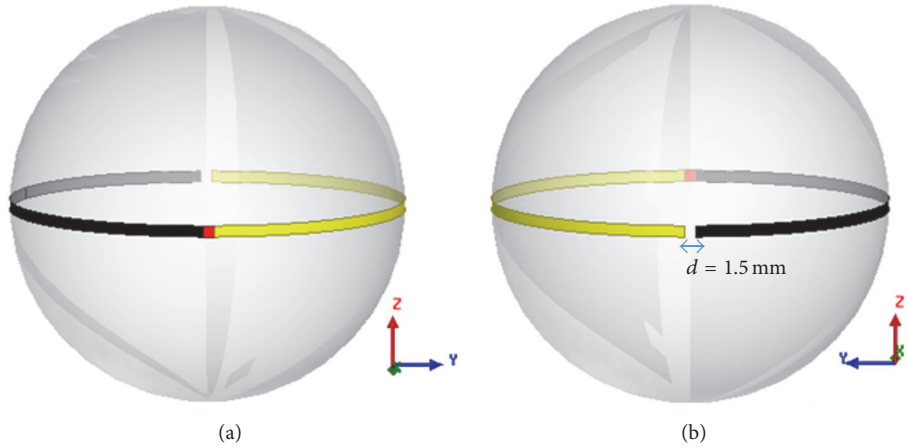

(a) (b)

Figure 2: Structure of the spherical 3D antenna (r = 26.34 mm): (a) front view and (b) back view.

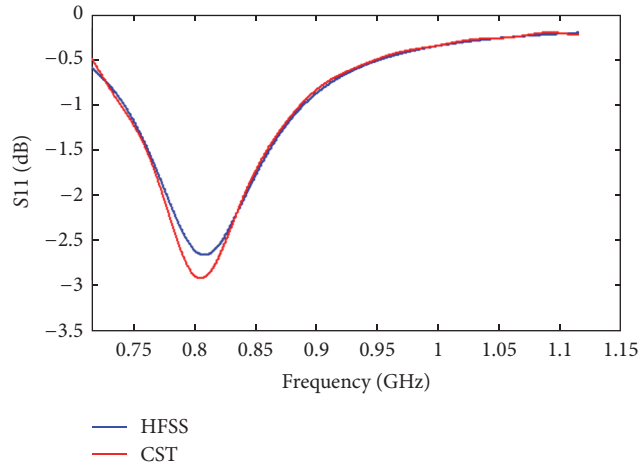

Figure 3: Return loss $S11$ of the 3D spherical antenna (Figure 2).

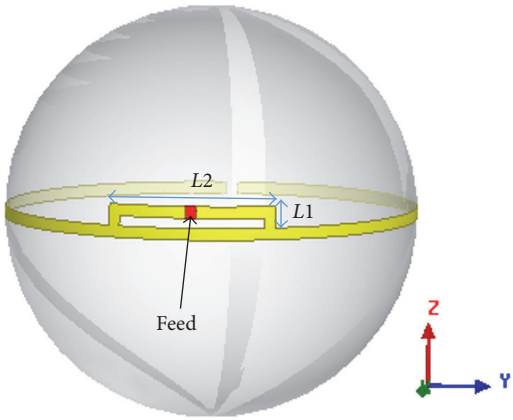

Figure 4: Structure of the 3D spherical antenna (Figure 2) with T-match.

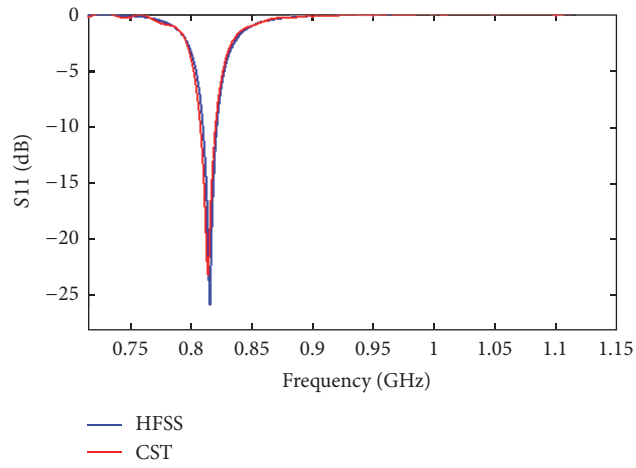

Figure 5: Return loss $S11$ of the 3D spherical antenna (Figure 4).

The new $S11$ of the antenna that is illustrated in Figure 5 has a minimum lower to −10 dB at a less than 915 MHz frequency. So, we will decrease the length D (Figure 6) to increase the operating frequency at 915 MHz.

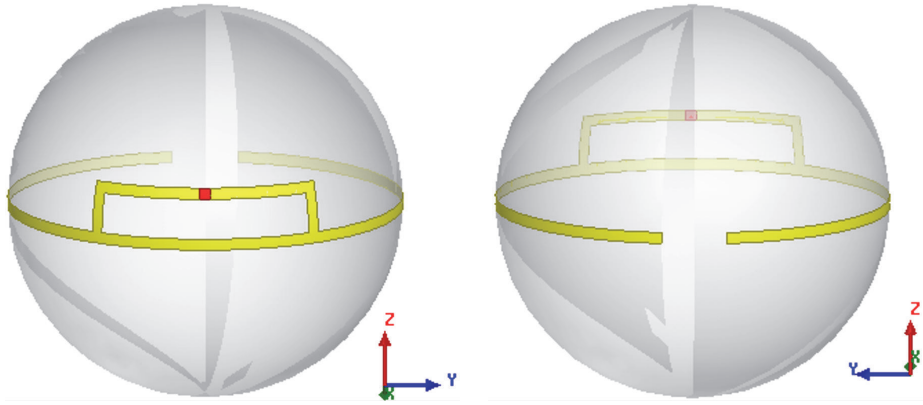

(a) (b)

Figure 6: Structure of the 3D spherical antenna with T-match: (a) front view and (b) back view.

Table 2: Dimensions of the 3D spherical antenna (Figure 6).

Parameters	r	D	$L1$	$L2$
Values (mm)	26.34	156.64	6.89	30.66

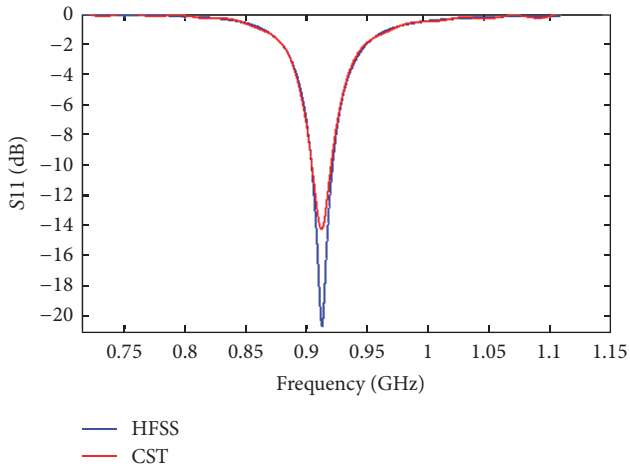

Figure 7: Return loss $S11$ of the 3D spherical antenna (Table 2).

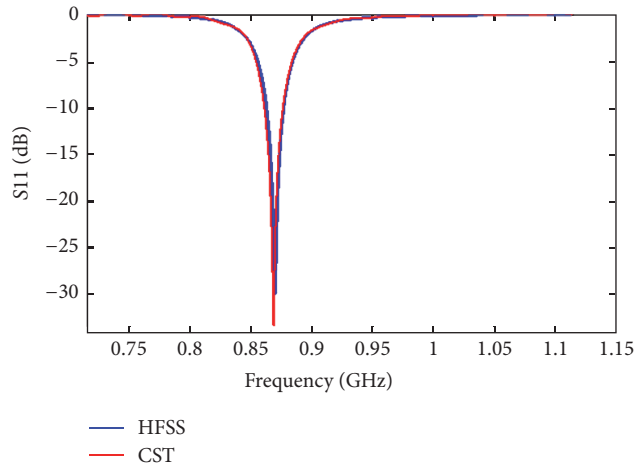

Figure 8: Return loss $S11$ of the 3D spherical antenna (Table 3).

Table 3: New dimensions of the 3D spherical antenna (Figure 4).

Parameters	r	D	$L1$	$L2$
Values (mm)	25.18	156.64	6.88	30.54

Table 2 illustrates the new dimensions of the 3D spherical antenna, which operates approximately in 915 MHz and has a $S11$ inferior to −10 dB as presented in Figure 7.

An antenna is electrically small when ka is less than 0.5. The electric size ka of this antenna is 0.5048 so we will decrease the radius r (in this case $a = r$) with the conservation of D until the separation distance $d = 1.5$ mm. The simulated $S11$ of the antenna is shown in Figure 8 and the dimensions of the antenna are mentioned in Table 3.

From the results, the antenna resonates at a frequency lower than the desired frequency (915 MHz) as before. So when we fix r and decrease D, the frequency increases, and if we do the opposite, the frequency decreases. So, we will at same time decrease D and r with always $d = 1.5$ mm until we find the limits of D and r so that the antenna operates approximately at 915 MHz. The final dimensions of the antenna and the results of $S11$ are mentioned in Table 4 and in Figure 9, respectively.

From the results of simulation of Figure 8, we found that,

(i) through HFSS, the $S11$ depending on the frequency reaches the level of −21 dB at a resonant frequency equal to 914.4 MHz,

(ii) through CST, the $S11$ depending on the frequency reaches the level of −33.48 dB at a resonant frequency equal to 914.7 MHz.

As these results shown, the antenna resonates approximately at 915 MHz, with a lower $S11$ than −10 dB.

Regarding the radiation pattern, Figure 10 shows the radiation patterns of the electric field total radiated (E_{total}) in dB of the antenna at 915 MHz in the three planes xz ($\phi = 0^\circ$), yz ($\phi = 90^\circ$), and xy ($\theta = 90^\circ$). According to these diagrams,

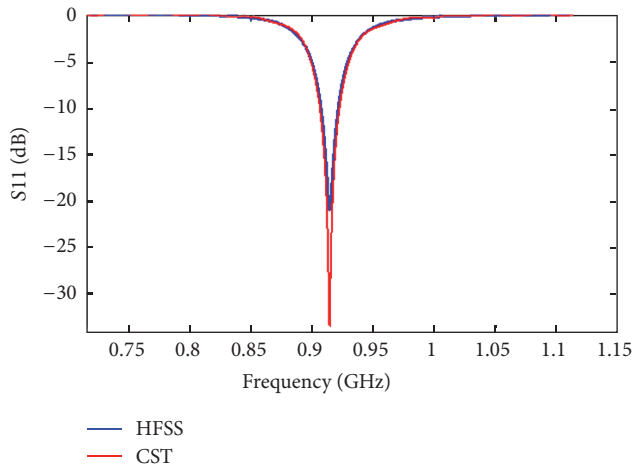

Figure 9: Return loss S11 of the 3D spherical antenna (Table 4).

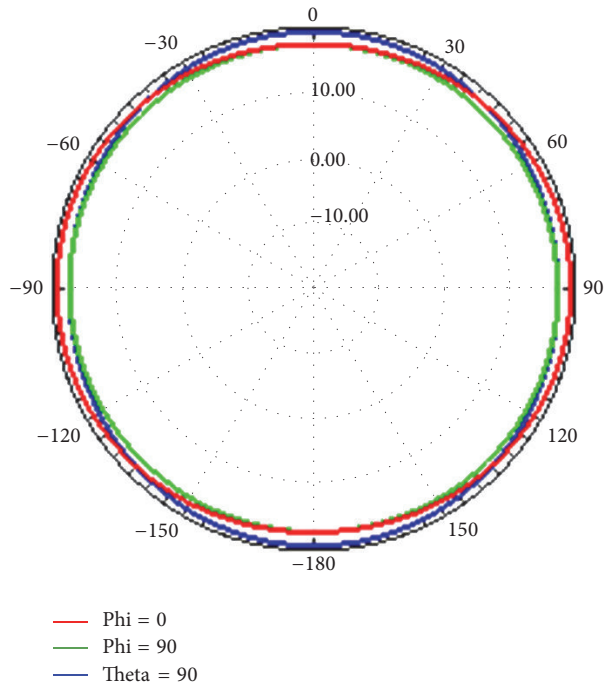

Figure 10: Radiation pattern (E_{total}) in 2D of the 3D spherical antenna (Table 4) in the planes: xz, yz, and xy.

Table 4: Final dimensions of the 3D spherical antenna (Figure 4).

Parameters	r	D	$L1$	$L2$
Values (mm)	23.9	148.94	6.86	30.39

the variation of E_{total} does not attain the zero in the three planes and we see it well in Figure 11 which represents the radiation patterns in all space (3D).

So, the radiation pattern becomes nearly isotropic because the two arms of the dipole are wound in the same direction of current along the axes x, y, and z as shown in Figure 12.

The antenna gain is also simulated, the maximum gain is 1.52 dBi, and the minimal is −0.68 dBi. Therefore, the gain is reduced to 2.2 dBi which is less than 3 dBi, which means that we have an opening angle of the antenna equal to 360° in all directions of space.

We can compare the antenna of this work with the antenna of the work presented in [12]. Table 5 summarizes simulation results obtained by HFSS of the two antennas.

From Table 5, the size of our antenna is small compared to the size of the antenna [12] which gives us a reduction in the electrical size of 8.03%. The resonant frequency of this antenna is very close to the desired frequency relative to [12]. The difference between the maximum gain and the minimum gain of this antenna is less than 3 dBi; on the

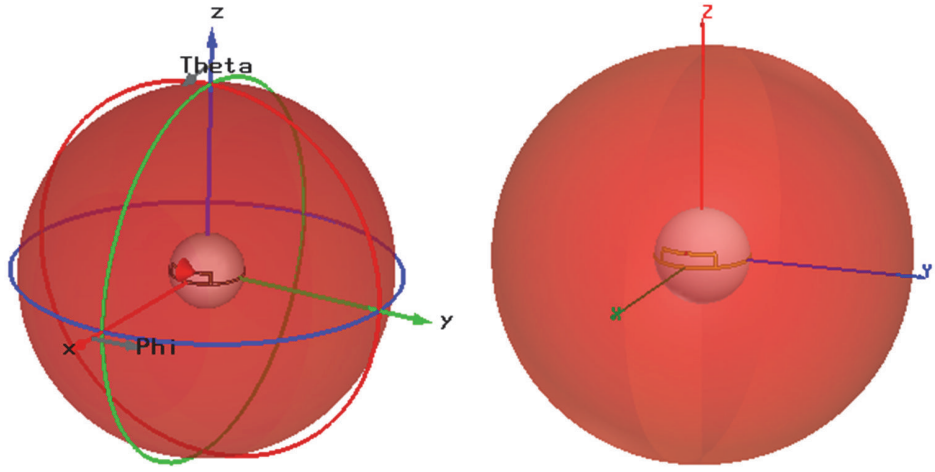

(a) (b)

Figure 11: Radiation patterns (E_{total}) in 3D of the 3D spherical antenna (Table 4): (a) simulated by CST and (b) simulated by HFSS.

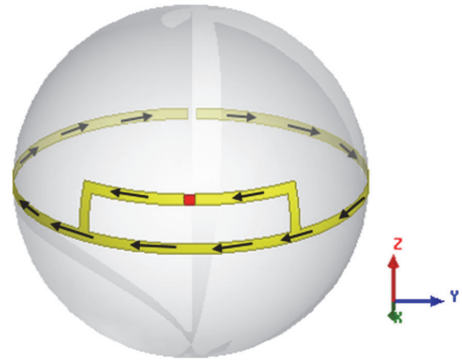

Figure 12: Current directions along the two arms of the 3D spherical antenna (Table 4).

Table 5: Comparison between this work and the work [12].

Antenna	Present	[12]
r (mm)	23.9	26
ka	0.458	0.498
Resonant frequency desired (MHz)	915	915
Resonance frequency obtained (MHz)	914.4	930
Gain_{Max} (dB)	1.52	1.81
Gain_{Min} (dB)	−0.68	−8.07
$\text{Gain}_{\text{Max}} - \text{Gain}_{\text{Min}}$ (dB)	2.2	9.88
Opening angle	360°	<360°

contrary, the difference of the gain of the antenna [12] is greater, which implies that our antenna has an opening angle of 360° independently of the direction of the space. Our results are relatively optimal than those found in the work [12].

If we continue the decrease of D and r, we will find that the resonance frequency is greater than the desired frequency, so, in the next section, we will fold the arms of dipole to minimize the size of the antenna.

2.2. 3D Spherical Antenna Based on a Folded Arms Dipole. In this design, we have reduced the electrical size of the antenna above by folding the arms in the opposite directions (Figure 13(a)) so that the two arms of the dipole are wound in the same direction of current (Figure 13(b)).

We will decrease the radius r from 22 mm to 14 mm with a step of 2 mm and the separation distance is always $d = 1.5$ mm. This reduction implies the reduction in D and the increase in $D1$ with fixed d so that the antenna operates at 915 MHz as shown in Figure 14. Table 6 lists the dimensions of each antenna ($r = 22$, $r = 20$, $r = 18$, $r = 16$, and $r = 14$ mm) with the simulation results of the $S11$ of each antenna simulated by HFSS (Figure 15).

According to the results, all the antennas resonate at a frequency that is close to the desired frequency 915 MHz with different bandwidth which varies proportionally to the size of each antenna.

The radiation patterns of E_{total} radiated (dB) of each antenna at 915 MHz in the three planes xz ($\phi = 0°$), yz ($\phi = 90°$), and xy ($\theta = 90°$) are shown in Figure 16.

According to Figure 16, the variation of E_{total} depending on r does not achieve the zero in the xz and xy planes, but in the yz plane, we see that the variation tends toward zero when

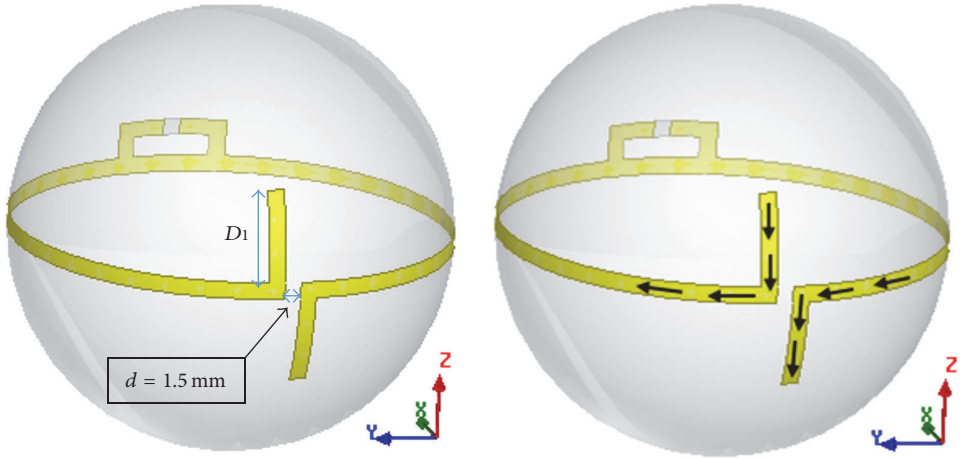

(a) (b)

Figure 13: (a) Structure of the 3D spherical antenna with folded arms and (b) current direction along the folded arms.

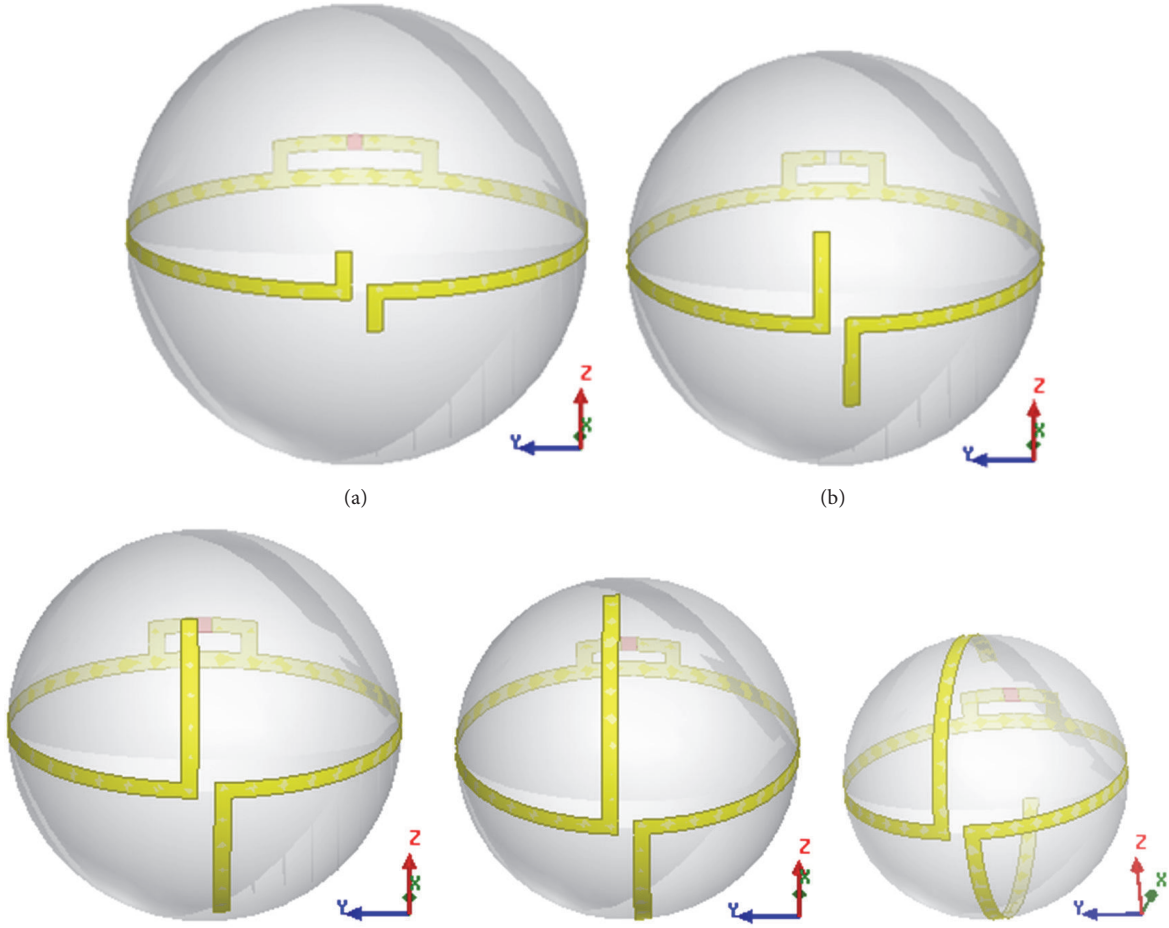

(a) (b)

(c) (d) (e)

Figure 14: Structure of 3D spherical antennas of different radius: (a) $r = 22$ mm, (b) $r = 20$ mm, (c) $r = 18$ mm, (d) $r = 16$ mm, and (e) $r = 14$ mm.

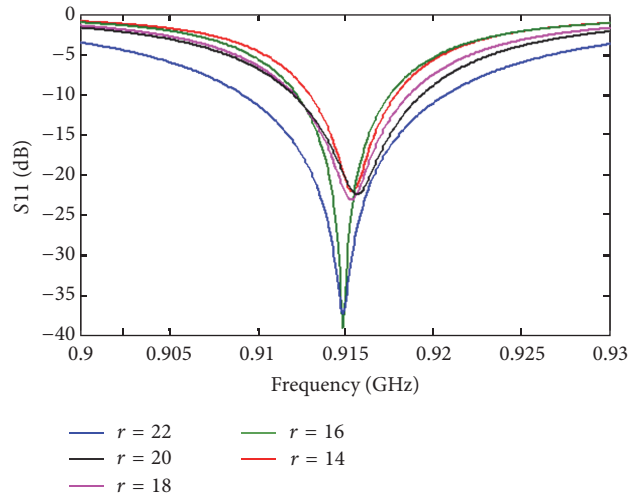

Figure 15: Return loss $S11$ of each 3D spherical antenna (Table 6).

Table 6: Dimensions of each antenna (Figure 14) with the results of the simulation.

Parameters	Values				
r (mm)	22	20	18	16	14
D (mm)	136.65	124.1	111.5	98.92	86.34
$D1$ (mm)	5.9	8.4	15.6	24.47	35.46
$L1$ (mm)	3.21	3.35	3.31	2.53	2.75
$L2$ (mm)	16	10	10	9.8	10
$S11$ (dB)	−36.52	−21.91	−22.6	−38.34	−21.63
fr (MHz)	914.9	915.7	915.4	914.9	915.4

Table 7: Dimensions of the 3D spherical antenna (Figure 18).

Parameters	r	D	$D1$	$D2$	$D3$	$L1$	$L2$
Values (mm)	14	81.74	7.83	4	18.09	3.23	6

Table 8: Dimensions of each 3D spherical antenna (Figure 18) with the simulation results.

Antenna	1	2	3	4
r (mm)	14	14	14	14
D (mm)	80.94	80.14	79.34	78.54
$D1$ (mm)	9.9	11.36	12.32	13.47
$D2$ (mm)	4	4	4	4
$D3$ (mm)	22.65	25.98	28.28	31.04
$L1$ (mm)	3.23	3.23	3.23	3.23
$L2$ (mm)	6	6	6	6
$S11$ (dB)	−28.89	−42.38	−38.08	−23
fr (MHz)	915	915.2	915	915
$E_{max} - E_{min}$ (dB)	3.892	3.382	3.044	2.856
Opening angle (°)	<360	<360	<360	360

the r decreases; this makes the radiation antenna no quasi-isotropic. To explain this, Figure 17 presents the radiation pattern in the whole space of two antennas (r = 22 mm and r = 14 mm).

From the results, we observe that the strong increase in $D1$ influences the radiation of the antenna. To cancel this influence, we will fold the length of the dipole $D1$ which leads to a meander line dipole.

2.3. 3D Spherical Antenna Based on a Meander Line Dipole. In this step, we have kept the radius of the previous antenna (r = 14 mm) and we have folded the two lengths $D1$ of the dipole as shown in Figure 18, so that the two arms of the dipole are wound in the same direction of current in order to find a quasi-isotropic radiation. Moreover, the dimensions of this antenna are listed in Table 7.

The $S11$ of the antenna has a minimum value <−10 dB at a frequency very close to 915 MHz as present Figure 19.

The variation of the E_{total} does not attain the zero in the three planes and in all spaces as presented in Figures 20 and 21.

The difference between the maximum and the minimum fields is 4.061 dB which is greater than 3 dB, which results in an antenna that has an aperture angle which is inferior to 360°. We will render the opening angle equal to 360° in all directions of space by the reduction in D, the increase in $D1$ and $D3$, and the conservation of $D2$. Table 8 shows the dimensions of each antenna with the simulation results of Figure 22 which shows the $S11$ simulated by HFSS and Figure 23 which shows the variation of E_{total} radiated in dB according to ϕ and θ in the xz, xy, and yz planes.

From the results of Table 8, antenna 4 produces a quasi-isotropic radiation with a difference between the maximum and minimum field equal to 2.856 dB which leads to an opening angle in each side equal to 360°. Regarding the $S11$, it has a minimum value of −23 db at 915 MHz. To achieve these results, the total length of the dipole has been increased from 135.58 mm (Table 7) to 169,56 mm (Table 8, antenna 4). So you must decrease this length in order to reduce the cost. Further, we have made several decreases and we found in the end that this length can be reduced by increase in $D2$ and decrease

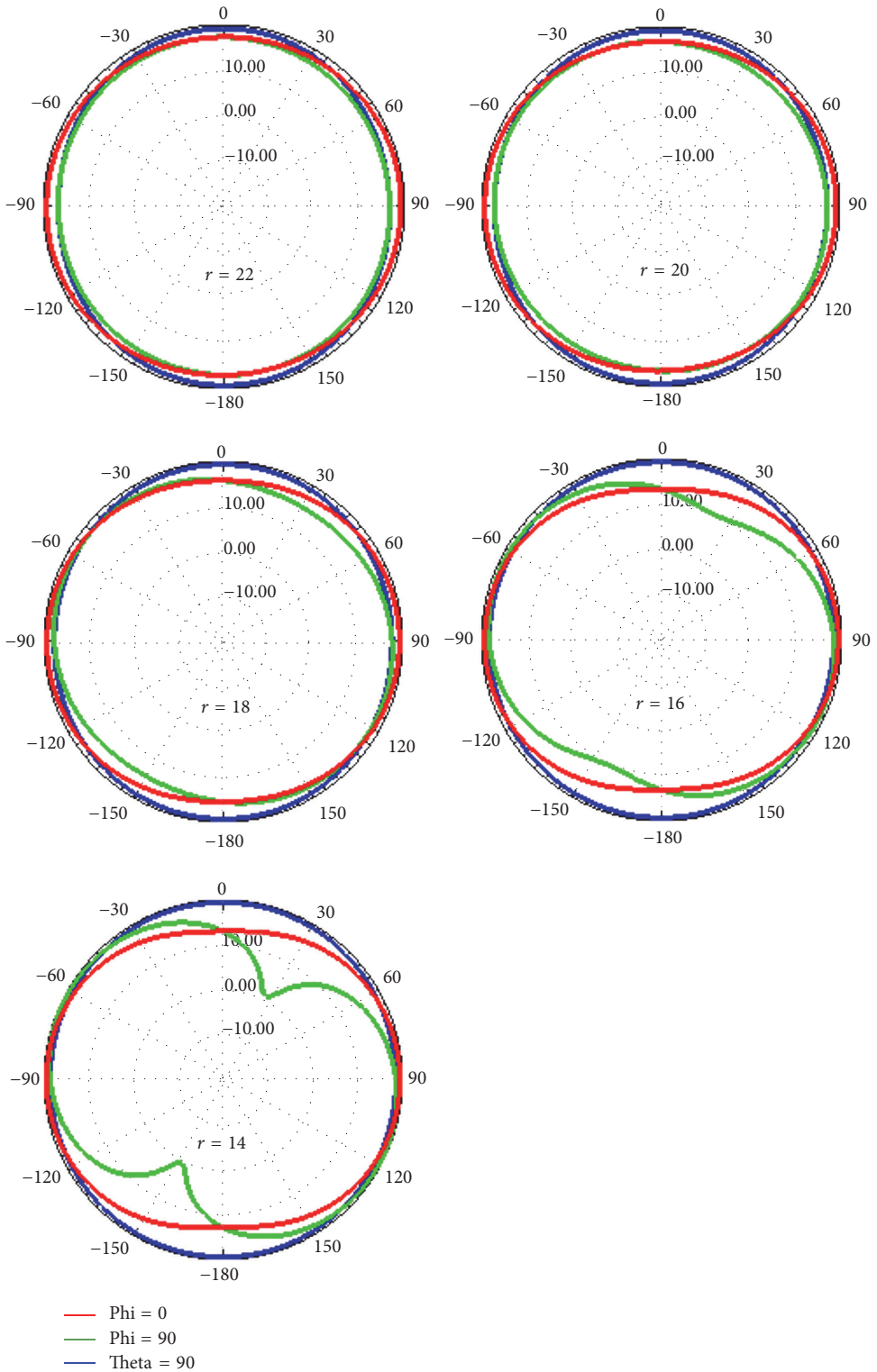

Figure 16: Radiation patterns (E_{total}) in 2D of each 3D spherical antenna (Table 6) in the planes: xz, yz, and xy.

in D, $D1$, and $D3$. Table 9 shows the dimensions of the four antennas with the simulation results of Figures 24 and 25.

We succeeded to reduce the total length of the dipole from 169.56 mm to 157.26 mm with the conservation of an opening angle equal to 360° in all the directions of space. The dipole total lengths of antenna 4 and antenna 3 are nearly equal which implies that we have achieved the limit of the reduction.

The electric size ka of the antenna is 0.2683. It exists in the literature that the antennas have lower ka. Therefore, we

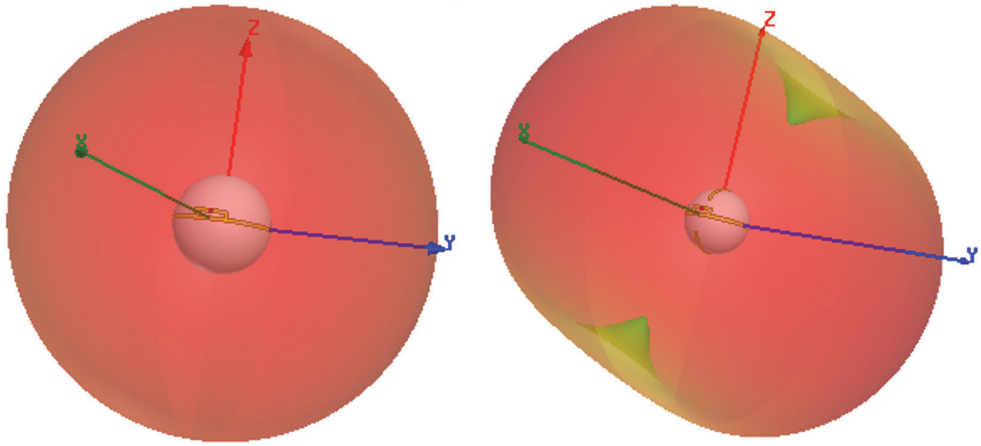

(a) (b)

Figure 17: Radiation patterns (E_{total}) in 3D of the 3D spherical antenna (Table 6): (a) $r = 22$ mm and (b) $r = 14$ mm.

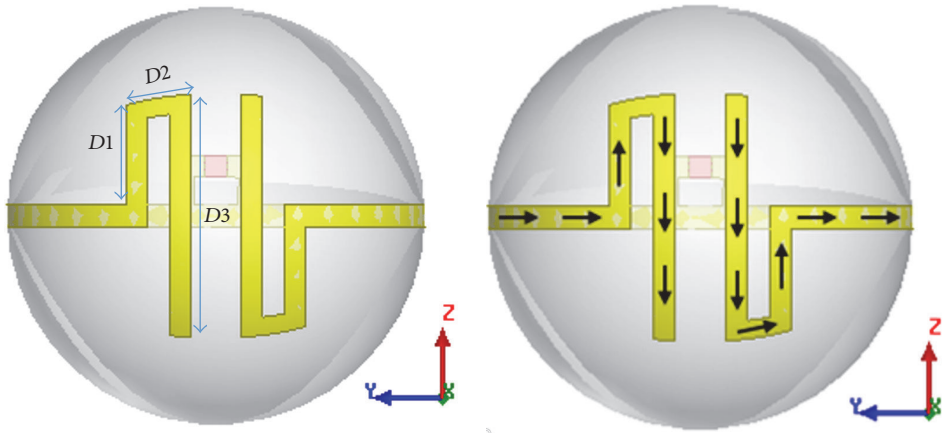

(a) (b)

Figure 18: (a) Structure of the 3D spherical antenna with meander line and (b) current direction along the *meander line dipole*.

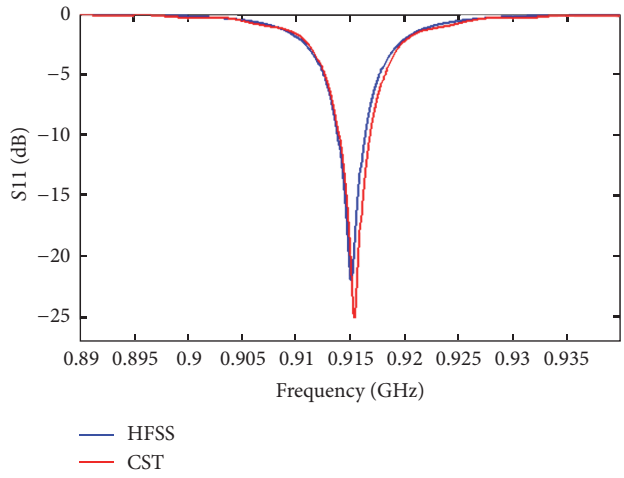

Figure 19: Return loss $S11$ of 3D spherical antenna (Table 7).

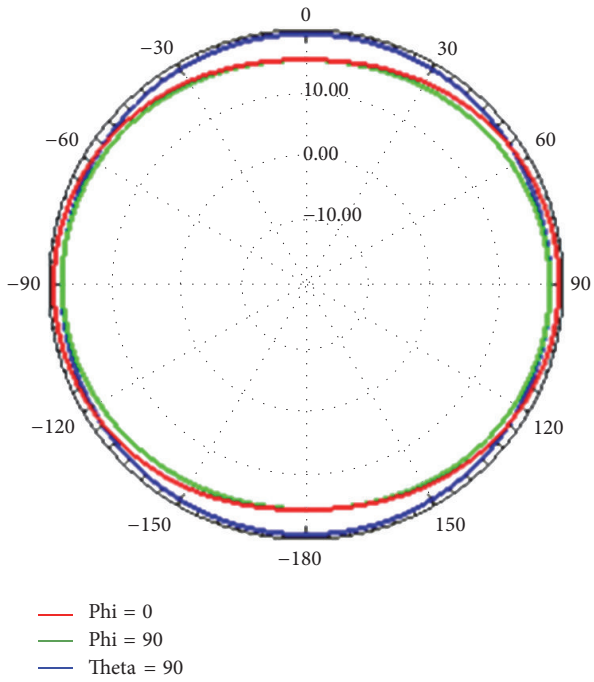

Figure 20: Radiation patterns (E_{total}) in 2D of 3D spherical antenna (Table 7) in the plans: xz, yz, and xy.

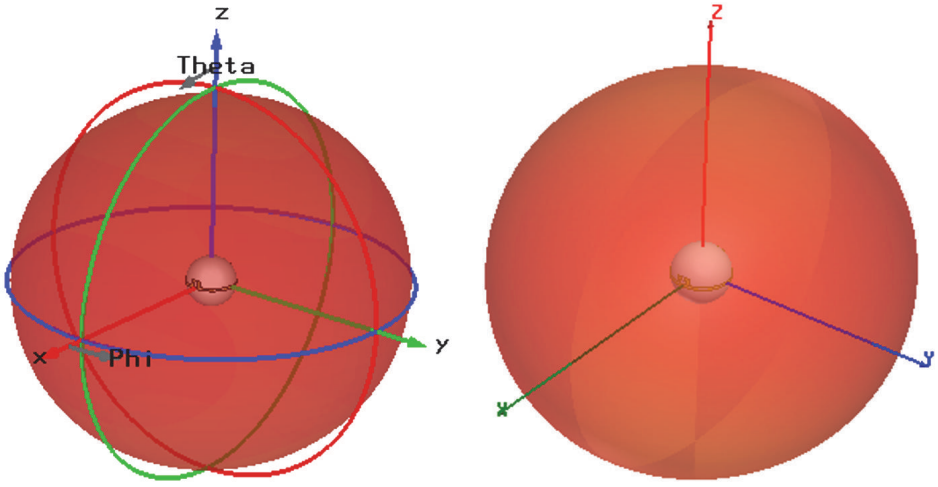

(a) (b)

Figure 21: Radiation patterns (E_{total}) in 3D of the 3D spherical antenna (Table 7): (a) CST and (b) HFSS.

will decrease ka (decrease of the radius r) based on previous parametric studies in order to obtain the 3D spherical antenna that has a small total length of dipole, operates at 915 MHz, and generates a quasi-isotropic radiation with an opening angle equal to 360° in each side. Table 10 shows the dimensions of the miniature antenna.

From the simulation results of Figure 26 which represents the $S11$ of this antenna, we have found that,

(i) through HFSS, the $S11$ depending on the frequency reaches the level of −22.53 dB at a resonant frequency equal to 915 MHz,

(ii) through CST, the $S11$ depending on the frequency reaches the level of −31.5 dB at a resonant frequency equal to 915.2 MHz.

From the results, the antenna resonates at a frequency near to 915 MHz with a level of $S11$ inferior to −10 dB.

Regarding the antenna radiation parameters, Figure 27 shows the radiation patterns of the E_{total} radiated (dB) in the three planes xz, yz, and xy. The variation of the field does not attain the zero in the three planes and in all space (Figure 28).

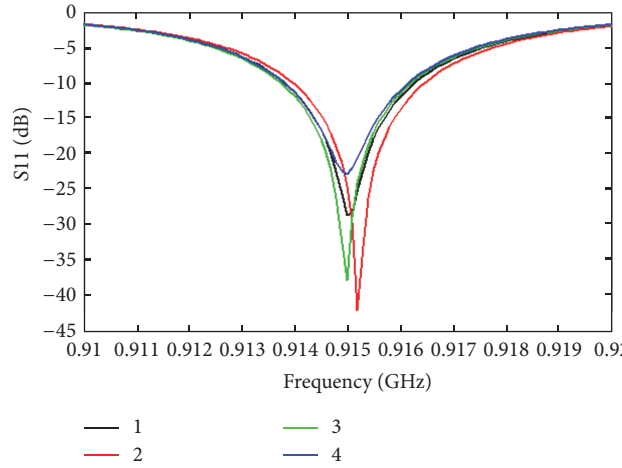

Figure 22: Return loss $S11$ of each 3D spherical antenna (Table 8).

Table 9: Dimensions of each 3D spherical antenna (Figure 18) with the simulation results.

Antenna	1	2	3	4
r (mm)	14	14	14	14
D (mm)	77.96	77.36	76,36	75.36
$D1$ (mm)	12.38	11.7	11.11	10.86
$D2$ (mm)	4.5	5	5.5	6
$D3$ (mm)	29.02	27.88	27.09	27.09
Total length (mm)	163.75	160.52	157.76	157.26
$L1$ (mm)	3.23	3.23	3.23	3.23
$L2$ (mm)	6	6	6	6
$S11$ (dB)	−28.09	−28.39	−26.44	−21.42
fr (MHz)	915.3	914.9	915.1	915.1
$E_{max} - E_{min}$ (dB)	2.58	2.815	2.816	2.835
Opening angle (°)	360	360	360	360

Table 10: Dimensions of the 3D spherical antenna (Figure 17).

Parameters	r	D	$D1$	$D2$	$D3$	$L1$	$L2$
Values (mm)	12	64.76	12.21	5.5	30.48	2.3	6

Table 11: Dimensions of the miniaturized 3D spherical antenna (Figure 18).

Parameters	r	D	$D1$	$D2$	$D3$	$L1$	$L2$
Values (mm)	10	54,16	13.14	5	33	2.43	4.5

The difference between the maximum and minimum field is 2.845 dB, which leads to an antenna producing a quasi-isotropic radiation with an opening angle equal to 360° in all directions.

The electric size ka of this antenna is 0.23, and after [13], their antenna has a ka equal to 0.24, which is close to ours. Therefore, we will further reduce the radius r to obtain a much miniaturized antenna size. Table 11 shows the dimensions of the miniaturized 3D spherical antenna.

Table 12: Comparison between this work and the previous work [13].

Antenna	Present	[13]
Radius (mm)	10	12.5
ka	0.1916	0.24
Total length (mm)	150.44	216
Resonant frequency desired (MHz)	915	911,25
Resonant frequency obtained (MHz)	915.1	912
$S11$ (dB)	−24.59	−15.9
Radiation pattern	Quasi-isotropic	Quasi-isotropic
Gain (dB)	1.264	0.75
Opening angle (°)	360	<360

From the results obtained by HFSS (Figure 29), the $S11$ reaches the level of −24.59 dB at a resonant frequency equal to 915.1 MHz, where $Z_a = 52.86 + j4.52\ \Omega$ at the same frequency. A minimum value $S11$ obtained by CST (Figure 29) is −20.91 dB at the 915.4 MHz, where $Z_a = 42.24 + j2.97\ \Omega$ at the same frequency.

The radiation parameters of this antenna are simulated at the frequency 915 MHz. Figure 30 shows the radiation pattern of E_{total} (dB) radiated in xz, xy, and yz planes. The E_{total} variation does not reach the zero in three planes and in all space as Figure 31 illustrates.

The difference between the maximum and minimum field is 2.72 dB. So, we have an antenna that produces a quasi-isotropic radiation with an opening angle equal to 360° in each side. The gain and the directivity of the antenna are also simulated; the maximum gain and directivity are, respectively, 1.264 dBi and 1.287 dBi which results in an efficiency of 98.21%.

The radius of the miniaturized 3D spherical antenna is equal to 10 mm which implies a dimension depending on the wavelength equal to $\lambda/32.78$. The antenna is classified as very small dimension referring to its electrical size $ka = 0.1916$ which is very less than 0.5.

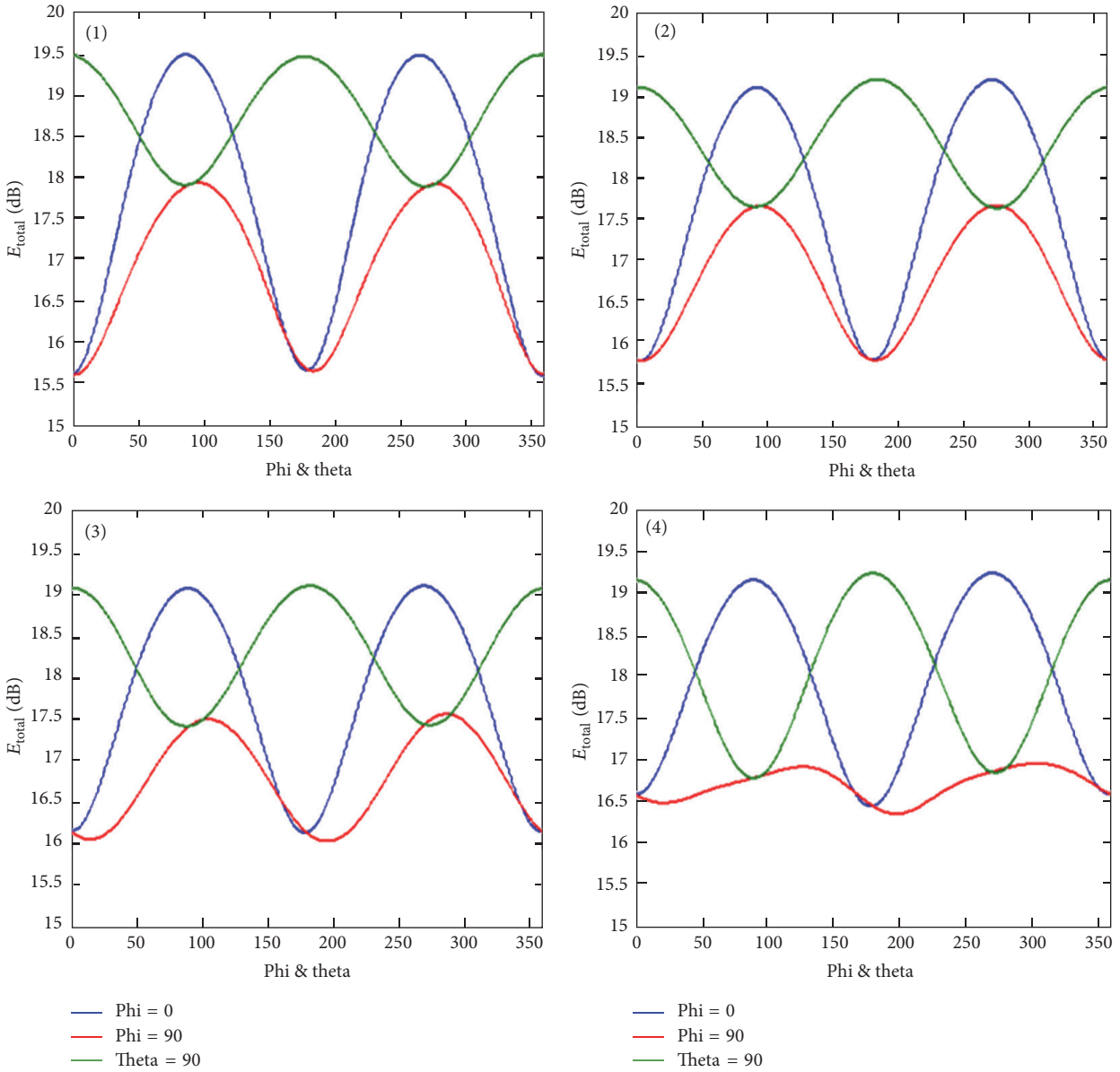

Figure 23: The E_{total} field of each 3D spherical antenna (Table 8) in the plans: xz, yz, and xy.

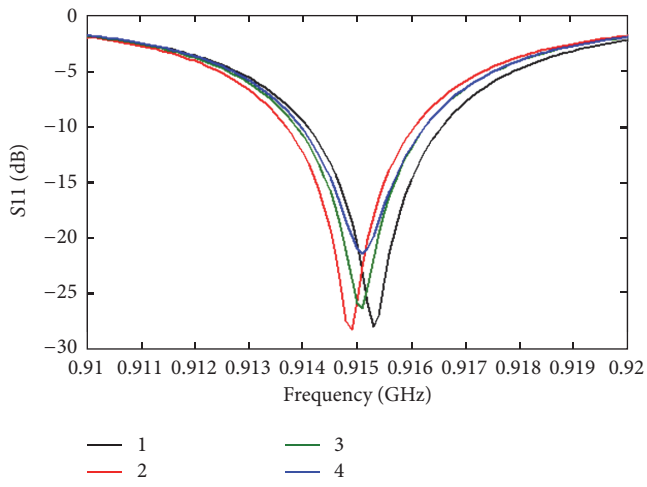

Figure 24: Return loss S11 of each 3D spherical antenna (Table 9).

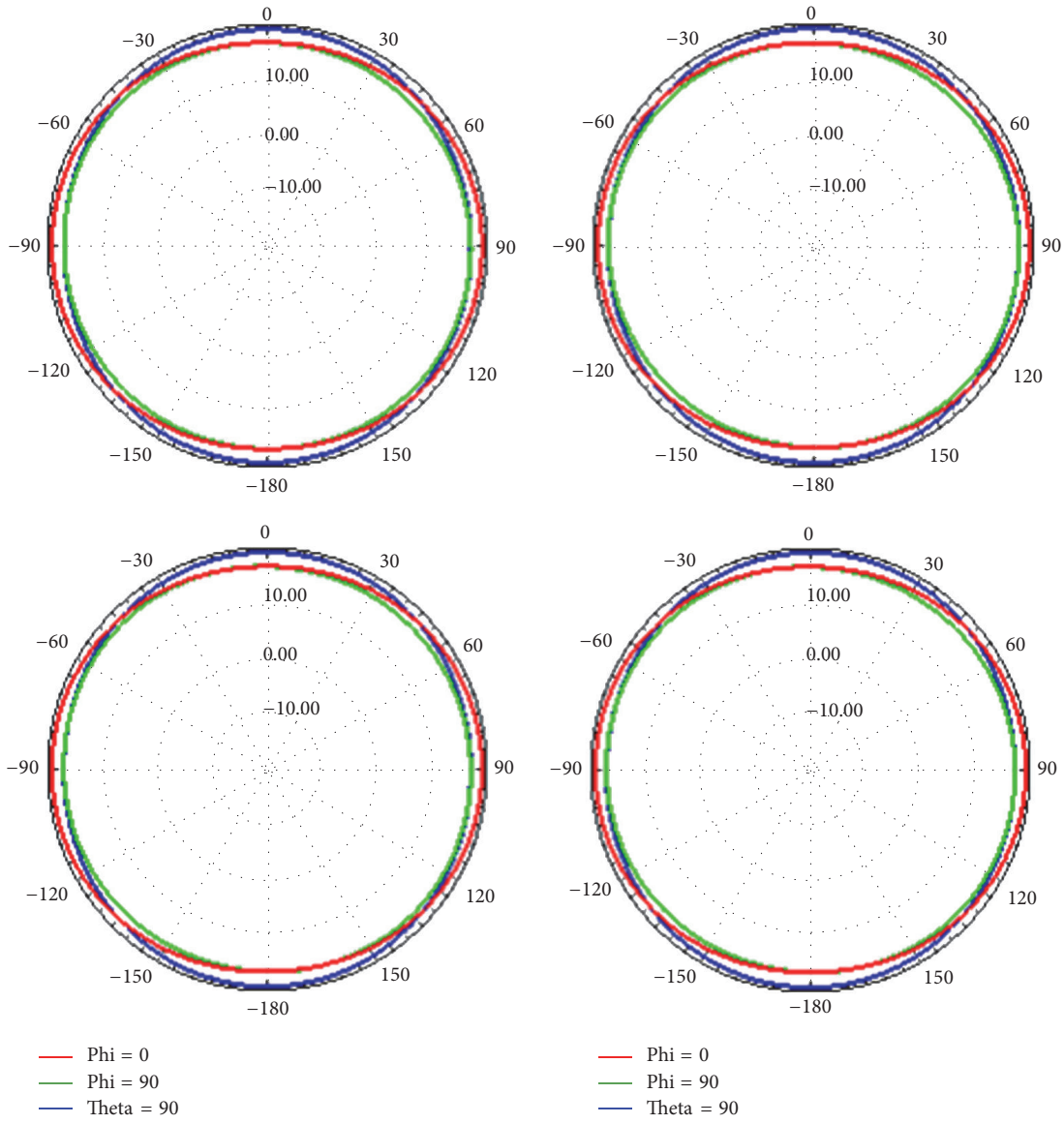

Figure 25: Radiation patterns (E_{total}) in 2D of each 3D spherical antenna (Table 9) in the plans: xz, yz, and xy.

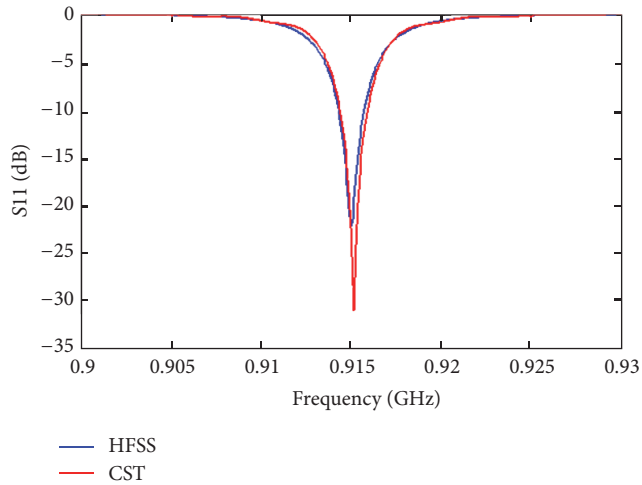

Figure 26: Return loss $S11$ of 3D spherical antenna (Table 10).

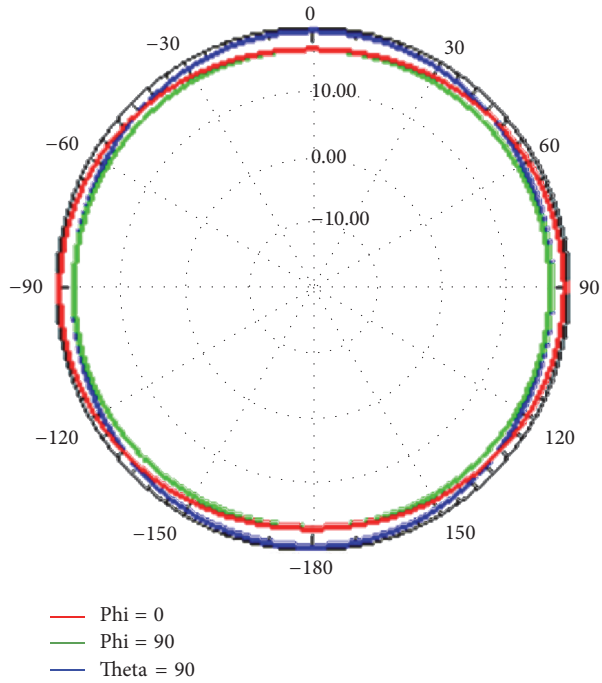

Figure 27: Radiation patterns (E_{total}) in 2D of 3D spherical antenna (Table 10) in the plans: xz, yz, and xy.

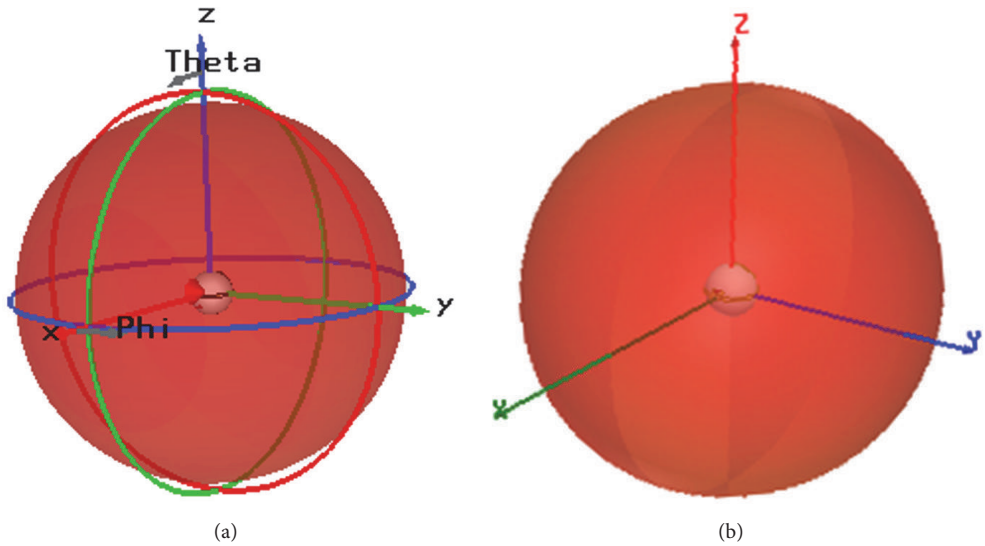

(a) (b)

Figure 28: Radiation patterns (E_{total}) in 3D of the 3D spherical antenna (Table 10): (a) CSE and (b) HFSS.

Regarding the polarization, Figure 32 shows the axial ratio (AR) of this antenna. The antenna polarization is circular in four areas where AR is equal to 1. When going from these four areas to the areas where RA is between 1 and 0, the polarization becomes elliptical and afterwards linear in areas where RA is equal to 0. So, we can say that the state of polarization of this antenna is heterogeneous.

To compare properly this work with the work of [13], Table 12 summarizes the antenna size with the simulation results that are obtained by HFSS.

From Table 12, the size of our antenna is smaller than the size of [13] which gives us a reduction in the electric size of 20.16% and a reduction of the volume of 48.8%. The resonant frequency of our antenna is very close to the desired frequency that is relative to [13]. The $S11$ levels depend on adaptation. The gain of the antenna of this work is higher than the gain of the antenna with 360° of an opening angle in the whole space [13].

These results are relatively optimal than those found in [13]. In addition, this antenna has advantages compared to

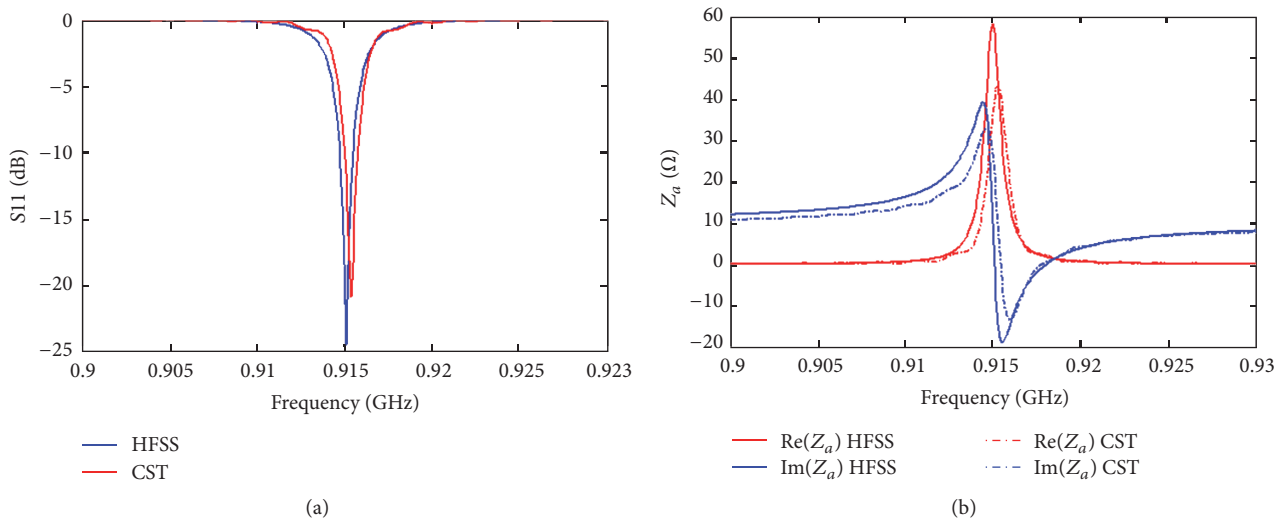

Figure 29: Circuit parameters of the 3D spherical antenna (Table 11): (a) return loss $S11$, (b) input impedance Z_a.

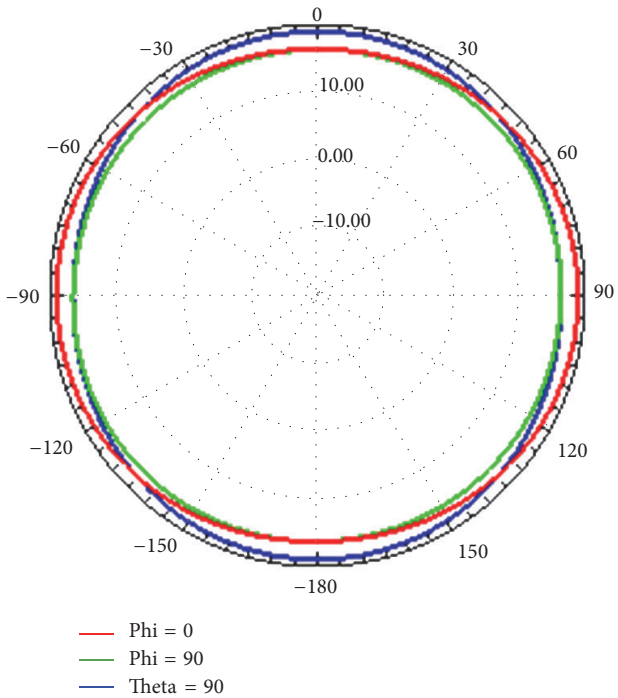

Figure 30: Radiation patterns (E_{total}) in 2D of 3D spherical antenna (Table 11) in the plans: xz, yz, and xy.

the antenna of [13] such as the reduced weight because we have used a Styrofoam sphere with 20 mm in diameter and 150.44 mm in total length of dipole. Similarly, the authors of [13] used the same sphere but its diameter is equal to 25 mm and the total length of dipole equal to 216 mm which also implies minimal manufacturing cost. We also have the advantage to obtain the compact size devices for RFID, WSN, and RSN applications because the size is very small and the shape of the antenna allows for placing the circuitry and sensors to its interior.

We can configure the antenna for many input impedance values Z_a [20] as well as for operating it at other frequencies by adjusting the geometric parameters.

3. Conclusion

The main goal of this work is to design an electrically small antenna on condition that it operates at a frequency of about 915 MHz and produces a quasi-isotropic radiation with an opening angle equal to 360° in all directions of space. For

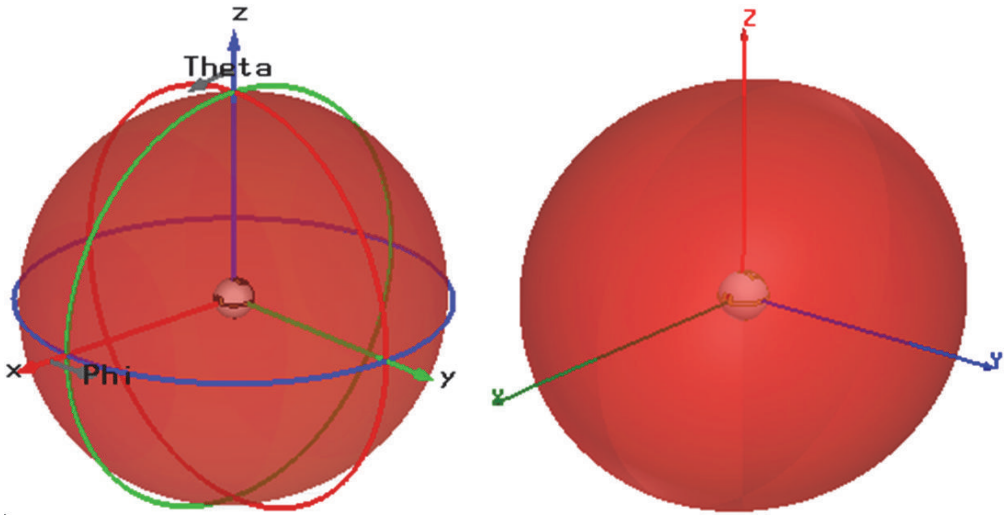

(a) (b)

Figure 31: Radiation patterns (E_{total}) in 3D of the 3D spherical antenna (Table 11): (a) CSE and (b) HFSS.

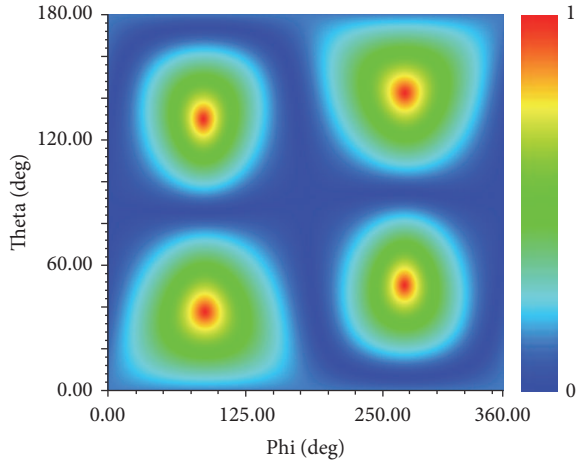

Figure 32: Axial ratio (AR) in linear scale of the 3D spherical antenna (Table 11).

this reason, we have first designed a spherical 3D antenna based on a linear dipole and the very small electrical size which can be found is $ka = 0.458$. Thus, we have decreased ka by folding the arms of the dipole. However, we have found the radiation of the antenna that becomes no quasi-isotropic only after a certain time during the decrease ka. In this case, we have folded the arms again as a meander line and we have obtained after the studies of geometric parameters a miniaturized 3D spherical antenna of electric size $ka = 0.1916$. From the simulation, we obtained a return loss $S11$ of −24.59 dB at 915.1 MHz, a quasi-isotropic radiation pattern with an opening angle equal to 360° in all directions of space, a maximum gain of 1.264 dBi, and an efficiency of 98.21%. This antenna has a very important role in RFID technology in the elimination the problem of unread tags and in WSN and RSN technologies by the elimination of intermittent communication between network nodes. In addition, this antenna has a shape that allows placing the sensor electronics in its interior which gives us compact devices.

Competing Interests

The authors declare that they have no competing interests.

References

[1] M. Bolic, D. Simplot-Ryl, and I. Stojmenović, *RFID Systems: Research Trends and Challenges*, John Wiley & Sons, Hoboken, NJ, USA, 2010.

[2] Q. Wang and I. Balasingham, *Wireless Sensor Networks—An Introduction, Wireless Sensor Networks: Application-Centric Design*, Edited by Y. K. Tan, InTech, 2010.

[3] H. Liu, M. Bolic, A. Nayak, and I. Stojmenović, "Taxonomy and challenges of the integration of RFID and wireless sensor networks," *IEEE Network*, vol. 22, no. 6, pp. 26–35, 2008.

[4] L. Zhang and Z. Wang, "Integration of RFID into wireless sensor networks: architectures, opportunities and challenging problems," in *Proceedings of the 5th International Conference on Grid and Cooperative Computing Workshops (GCC '06)*, pp. 463–469, IEEE, Hunan, China, October 2006.

[5] A. Mitrokotsa and C. Douligeris, "Integrated RFID and sensor networks: architectures and applications," in *RFID and Sensor Networks: Architectures, Protocols, Security and Integrations*, pp. 511–535, CRC Press, 2009.

[6] B. Zhang, K. Hu, and Y. Zhu, "Network architecture and energy analysis of the integration of RFID and wireless sensor network," in *Proceedings of the Chinese Control and Decision Conference (CCDC '10)*, pp. 1379–1382, May 2010.

[7] F. M. Al-Turjman, A. E. Al-Fagih, and H. S. Hassanein, "A novel cost-effective architecture and deployment strategy for integrated RFID and WSN systems," in *Proceedings of the International Conference on Computing, Networking and Communications (ICNC '12)*, pp. 835–839, Maui, Hawaii, USA, January 2012.

[8] M. J. Cazeca, J. Mead, J. Chen, and R. Nagarajan, "Passive wireless displacement sensor based on RFID technology," *Sensors and Actuators A: Physical*, vol. 190, pp. 197–202, 2013.

[9] A. Oprea, N. Bârsan, U. Weimar, M.-L. Bauersfeld, D. Ebling, and J. Wöllenstein, "Capacitive humidity sensors on flexible RFID labels," *Sensors and Actuators, B: Chemical*, vol. 132, no. 2, pp. 404–410, 2008.

[10] A. Babar, L. Ukkonen, and L. Sydanheimo, "Dual UHF RFID band miniaturized multipurpose planar antenna for compact wireless systems," in *Proceedings of the International Workshop on Antenna Technology: Small Antennas, Innovative Structures and Materials (iWAT '10)*, pp. 1–4, March 2010.

[11] R. H. Bhuiyan, R. Dougal, and M. Ali, "A new crossed staircase dipole antenna for 915 MHz RFID application," in *Proceedings of the IEEE Antennas and Propagation Society International Symposium (AP-S '08)*, pp. 1–4, July 2008.

[12] L. A. Berge and M. T. Reich, "A UHF RFID antenna for a wireless sensor platform with a near-isotropic radiation pattern," in *Proceedings of the IEEE International Conference on RFID (RFID '13)*, pp. 88–95, IEEE, Penang, Malaysia, May 2013.

[13] H.-K. Ryu, G. Jung, D.-K. Ju, S. Lim, and J.-M. Woo, "An electrically small spherical UHF RFID tag antenna with quasi-isotropic patterns for wireless sensor networks," *IEEE Antennas and Wireless Propagation Letters*, vol. 9, pp. 60–62, 2010.

[14] A. Bou-El-Harmel, A. Benbassou, and J. Belkadid, "Design of a three-dimensional antenna UHF in the form cubic intended for RFID, wireless sensor networks (WSNs) and RFID sensor networks (RSNs) applications," *International Journal on Communications Antenna and Propagation*, vol. 4, no. 6, pp. 260–264, 2014.

[15] A. Bou-El-Harmel, A. Benbassou, and J. Belkadid, "Optimization of a 3D UHF cubic antenna with quasi-isotropic radiation pattern for RFID, WSN and RSN applications," *WSEAS Transactions on Communications*, vol. 14, no. 42, pp. 365–373, 2015.

[16] B. R. Foster and R. A. Burberry, "Antenna problems in RFID systems," in *IEE Colloquium on RFID Technology*, Ref. No.1999/123, pp. 3/1–3/5, 1999.

[17] P. V. Nikitin and K. V. S. Rao, "Performance limitations of passive UHF RFID systems," in *Proceedings of the IEEE Antennas and Propagation Society International Symposium (APS '06)*, pp. 1011–1014, IEEE, Albuquerque, NM, USA, July 2006.

[18] Symbol Technologies Inc, "Two RF inputs makes a betterRFID tag," http://www.symbol.com/category.php?fileName=AB-26_2_inputs-better_rfid_tag.xml.

[19] S. R. Best, "A study of the performance properties of small antennas," in *Proceedings of the Antenna Applications Symposium*, pp. 193–219, Monticello, Ill, USA, September 2007.

[20] G. Marrocco, "The art of UHF RFID antenna design: impedance-matching and size-reduction techniques," *IEEE Antennas and Propagation Magazine*, vol. 50, no. 1, pp. 66–79, 2008.